Dopant-induced stabilization of rhombohedral $LiMnO_2$ against Jahn-Teller distortion

R. Prasad
Department of Physics, Indian Institute of Technology at Kanpur, Kanpur, India 208016

R. Benedek and M. M. Thackeray
Chemical Engineering Division, Argonne National Laboratory, Argonne, Illinois, 60439, USA
(Received 7 December 2004; published 29 April 2005)

Dopants introduced into layered $LiMnO_2$, a candidate cathode material for lithium batteries, tend to suppress the Jahn-Teller-effect-driven monoclinic distortion (symmetry $C2/m$) in favor of the layered rhombohedral structure ($R\bar{3}m$), which has superior Li insertion/extraction cycling properties. First-principles calculations, within the Local-Spin-Density-Approximation Generalized-Gradient-Approximation (LSDA-GGA) framework, implemented in the VASP code, are performed for 3*d* transition-metal, as well as Mg, Zn, Al, and N dopants, in order to assess their relative effectiveness in stabilizing the $R\bar{3}m$ symmetry. At the concentration $x=0.25$, the selected cation dopants (with the exception of Co and Fe) are found to adopt the same oxidation state (divalent or trivalent) in both monoclinic and rhombohedral structures. Transition metals earlier than Fe are trivalent, whereas those later than Co are divalent. Co in monoclinic $LiMnO_2$ exhibits (stable) trivalent and (metastable) divalent states that are only narrowly different in energy. Fe is trivalent in the monoclinic structure, but is mixed valent in the rhombohedral structure. Divalent dopants (which oxidize a neighboring Mn to the [non-Jahn-Teller-active] 4+ oxidation state) promote rhombohedral structure stabilization to a greater extent than trivalent dopants. Within the class of divalent dopants, the filled shell systems Mg and Zn are more effective than those with partially filled e_g shells. Within the class of trivalent dopants, those with partially filled t_{2g} shells are more effective than those with filled or empty shells. Breathing mode (Q_1) and Jahn-Teller active (Q_2, Q_3) phonon coordinates of transition metal octahedra are analyzed.

DOI: 10.1103/PhysRevB.71.134111 PACS number(s): 61.66.Fn

I. INTRODUCTION

The standard cathode material in commercial lithium batteries[1] is $LiCoO_2$. It would be desirable, from the standpoint of cost, toxicity and safety, to replace Co, or at least reduce its concentration, and Mn is an attractive candidate to substitute for Co. The stable form of $LiMnO_2$, however, is orthorhombic,[2] with symmetry *Pmmn*, a less favorable structure for lithium insertion/extraction cycling than the layered rhombohedral ($R\bar{3}m$) structure of lithium cobaltate, which has a higher symmetry. Nevertheless, a metastable layered form of $LiMnO_2$ does exist and can be synthesized by ion exchange in $NaMnO_2$.[3,4] The Jahn-Teller activity of Mn^{3+} in this compound results in a cooperative monoclinic distortion that is absent from most compounds with composition $LiMO_2$ (where $M=V,Co,Ni$) that adopt the α-$NaFeO_2$ structure. However, doping, for example with Co,[5] suppresses the monoclinic distortion in favor of the $R\bar{3}m$ symmetry. Other dopants in layered $LiMnO_2$ have also been studied experimentally.[6–9]

To guide future materials design, it is of interest to characterize the properties of dopants in candidate cathode materials. Since the experimental synthesis of homogeneous single-phase specimens is often difficult in practice, computer simulation offers an attractive alternative to elucidate trends in the behavior of selected dopants. Although practical implementations of the first-principles approach based on density functional theory are approximate, particularly in regard to calculated energy gaps and electronic quasiparticle spectra, they do yield accurate predictions of structural properties for most materials.

In an earlier article,[10] we presented first-principles calculations for Co impurities in layered $LiMn_{1-x}M_xO_2$. It was found that Co adopts a divalent state, which suppresses the cooperative Jahn-Teller distortion by oxidizing Mn-atom neighbors to the 4+ state. In this article, several other possible dopants are addressed. Incidentally, our discussion here is restricted to fully-lithiated stoichiometries, although the transformation from rhombohedral (layered) to cubic spinel that occurs upon delithiation of $LiMn_{1-x}M_xO_2$ is an important consideration for cathode design.[11,12]

In the simplest picture, a dopant tends to destabilize (stabilize) the monoclinic (rhombohedral) structure by diluting the number of Jahn-Teller active Mn^{3+} sites by one (the site of substitution) in the case of a trivalent dopant and two (the site of substitution and the site of the neighboring Mn^{4+}) in the case of a divalent dopant. To test this picture, the oxidation state of a given dopant must be determined. Our analysis indicates that the relatively early transition element dopants Sc, Ti, V, and Cr are trivalent, the later ones Ni and Cu are divalent, and Fe and Co show mixed-valent character with a higher oxidation state in the monoclinic than in rhombohedral structure.

The results of this work indicate that divalent dopants are, as expected, the most effective in stabilizing the rhombohedral structure against a cooperative Jahn-Teller distortion. Within the class of trivalent (divalent) dopants, the stabilizing ability of the dopant depends on the filling of the t_{2g} (e_g) shell.

II. METHOD

Calculations were performed with the VASP code,[13] which implements the local-spin-density-functional approximation (LSDA) of density-functional theory in the ultrasoft pseudopotential representation, with a plane wave basis. We employ the generalized gradient approximation (GGA) correction[14] to LSDA, which was found[15] to give improved accuracy for Mn-oxides, compared with the LSDA. Recent work has demonstrated that greater accuracy for electronic and magnetic properties,[16], as well as electrochemical properties[17] relative to the LSDA-GGA, can be achieved with the LSDA+U (or GGA+U) approximation, which accounts for the on-site Coulomb interaction by penalizing partial occupancy of atomic *d*-states on the transition-metal sublattice. For atomic structure calculations, however, LSDA-GGA often yields respectable accuracy, even though the predicted spectral positions of the occupied transition metal *d*-bands relative to the oxygen *p*-bands tend to be too high.

Most of the present calculations were performed using 16-atom supercells for rhombohedral or monoclinic structure with $R\bar{3}m$ and $C2/m$ symmetry, respectively. Some test calculations on cells with 32 and 64 atoms were also performed. To make the calculations more tractable, idealized magnetic structures are assumed.

A. Dopants

We consider the first transition series, as well as Mg, Zn, and Al, as dopants on the transition-metal sublattice. N dopants on the oxygen sublattice are also considered. Most of the doped systems are treated at a concentration of 0.25. Naturally, there is no guarantee that solubility for all of the above dopants is achievable in practice at that level, but experiment[6–9] indicates that at least some of these dopants have a range of solubility in layered $LiMnO_2$.

B. Magnetic structure

Neutron diffraction measurements on orthorhombic $LiMnO_2$ reveal a commensurate antiferromagnetic structure[18] below the Neel temperature $T_N=261.5$, with alternating up and down spins along Mn atomic chains (Mn-Mn spacing approximately 2.8 Å) parallel to the monoclinic *b*-axis. That the ground state of layered monoclinic $LiMnO_2$ exhibits antiferromagnetic chains along close-packed atomic rows, analogous to the orthorhombic system, has not been verified experimentally. However, first-principles calculations[19] suggest that such a structure is at least relatively favorable energetically. For simplicity, the magnetic structure proposed by Singh (designated AF3) will be assumed in the present work. Incidentally, several lithiated Mn-oxides, such as Li—Mn spinels,[20–23] which have the additional complication of mixed valence, exhibit complex incommensurate magnetic structures, and are therefore more difficult to model, despite their technological significance.

Rhombohedral $LiMn_{1-x}M_xO_2$, in which the cooperative Jahn-Teller distortion is suppressed by a concentration *x* of dopant *M*, is assumed ferromagnetic in this work. Ferromagnetic behavior has been observed in the Ni-doped system at low temperatures.[24] The assumption of ferromagnetism in rhombohedral $LiMn_{1-x}M_xO_2$ restricts the consideration to relatively small *x*; $LiCrO_2$ is antiferromagnetic,[25] and $LiAlO_2$ and $LiFeO_2$ favor nonlayered structures.[26,27]

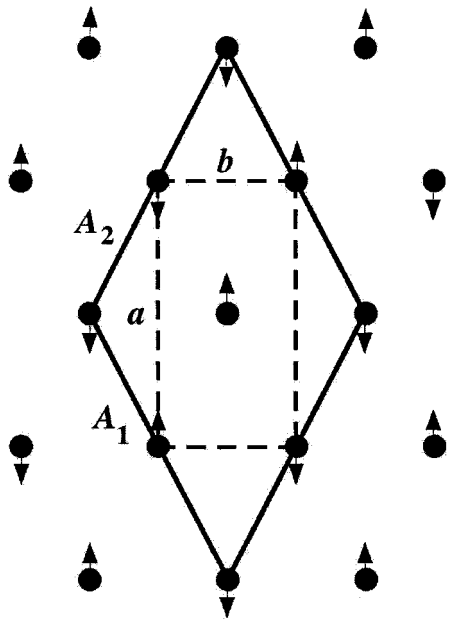

FIG. 1. Filled circles denote atomic positions in a single layer of the monoclinic structure of $LiMnO_2$. Dashed lines represent the primitive unit cell, and solid lines, the magnetic unit cell for a simple antiferromagnetic spin configuration. Up and down arrows represent oppositely directed Mn spins in the Mn layers.

C. Monoclinic crystal structure

The nonmagnetic primitive unit cell of monoclinic $LiMnO_2$ ($C2/m$ symmetry) contains two formula units. The experimentally observed lattice constants[5] are $a_m=5.44$ Å, $b_m=2.81$ Å, $c_m=5.39$ Å, and the monoclinic angle $\beta=116°$. (For simplicity, the subscript *m*, which denotes the monoclinic structure, will be omitted in the following equations.) A (nonprimitive) magnetic unit cell, with four formula units, can be constructed with basis vectors

$$\mathbf{A}_1=\mathbf{a}+\mathbf{b},\quad \mathbf{A}_2=\mathbf{b}-\mathbf{a},\quad \mathbf{A}_3=\mathbf{c}. \tag{1}$$

This choice is convenient, because four-formula-unit cells will be employed in most of the calculations presented for both monoclinic and rhombohedral structures. In the limiting case of $a/b=\sqrt{3}$, the *ab* (or A_1A_2) plane layers become hexagonal, and the cell lattice constants $A_1=A_2=2b$ are twice those of the primitive hexagonal layer unit cell. For the lattice constants quoted above for the monoclinic structure, the ratio $a/b=1.94$, about 12 percent larger than for the hexagonal cell. The (a,b) and (A_1,A_2) unit cells are illustrated in Fig. 1.

In the AF3 magnetic structure,[19] the spins along the A_2 axis are ordered ferromagnetically, and those along the A_1 axis, antiferromagnetically, as illustrated schematically by the upward and downward pointing arrows in Fig. 1. The magnetic (A_1,A_2) cell contains four formula units, and each

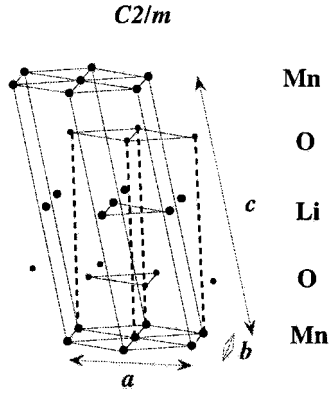

FIG. 2. The atomic structure of monoclinic $LiMnO_2$. Each layer has the structure illustrated in Fig. 1. The primitive cell lattice vectors *a*, *b*, and *c* are indicated. The dashed lines connect corresponding atomic positions in the first and fourth layers. In the limiting case in which the monoclinic (cooperative Jahn-Teller) distortion vanishes, the dashed lines are parallel to the hexagonal *c* axis, and correspond to the vertical lines in Fig. 3.

layer of Li, Mn, or O contains four atoms. If we consider a cell in which a Mn layer intersects the origin (layer $l=0$), a possible basis for this layer is given by the coordinates $(0,0,0)$, $(\frac{1}{2},0,0)$, $(0,\frac{1}{2},0)$, and $(\frac{1}{2},\frac{1}{2},0)$, where the components r_i in (r_1,r_2,r_3) are in units of A_i, $i=1,3$. The adjacent Li layer (layer $l=2$) sites are obtained by a displacement of $(\frac{1}{4},\frac{1}{4},\frac{1}{2})$, relative to the Mn atoms. The oxygen layers ($l=1,3$) consist of $4i$ sites sandwiched between Mn and Li layers, the coordinates of which have two internal degrees of freedom, *x* and *z*. If the coordinates of one of the sites are $\mathbf{r}(1)=(x,0,z)$, then the eight oxygen-site coordinates for layers $l=2,4$ in the (A_1,A_2,A_3) coordinate system can be expressed in the form

$$\mathbf{r}(j)=\mathrm{sgn}(j)\mathbf{r}(1)+n_1(j)\left(\tfrac{1}{2},0,0\right)+n_2(j)\left(0,\tfrac{1}{2},0\right), \qquad (2)$$

where $\mathrm{sgn}(j)$ is +1 or −1 when *j* is odd or even, and $n_1(j)$ and $n_2(j)$ are either 0 or 1. The internal parameters $x=0.2723$ and $z=0.7706$ were obtained by Armstrong *et al.*[5] An illustration of the layer stacking of monoclinic $LiMnO_2$ appears in Fig. 2.

Considering the prominence of the *b*-axis atomic chains in the monoclinic structure, it would be desirable to model doped systems by designing cells with an identical dopant concentration *x* in each individual chain, not merely in the cell as a whole. To do so for concentration $x=0.25$, however, would require at least an eight-formula unit cell, with two chains of four atoms each per layer. Better still would be 16 formula units, in view of the high aspect ratio of the eight formula unit cell. Although we have run tests on these larger cells, most of the calculations were performed on the four-formula-unit cells to avoid much larger computational costs. The main trends appear robust and would undoubtedly survive in larger-cell calculations.

D. Rhombohedral crystal structure

The layered rhombohedral (α-$NaFeO_2$) structure, with symmetry $R\bar{3}m$, is designated $O3$ in the classification of Delmas,[28] which refers to the octahedral coordination of the cations and its stacking periodicity. It is easiest to visualize in terms of hexagonal coordinates. A primitive cell can be generated with cell unit vectors

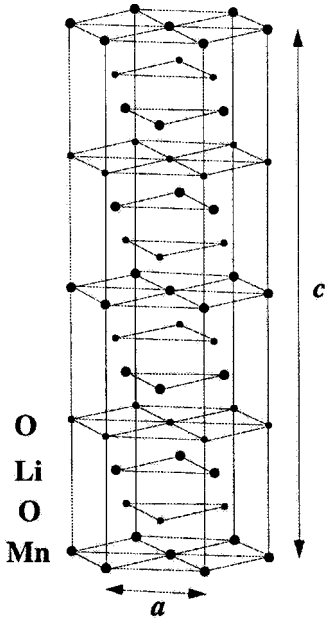

FIG. 3. Atomic structure of rhombohedral layered system of the α-$NaFeO_2$ type. The conventional hexagonal unit cell, with 12 atomic layers is illustrated; the primitive cell contains four layers.

$$\mathbf{B}_1^p=a_h\hat{\mathbf{i}}, \quad \mathbf{B}_2^p=-\frac{1}{2}a_h\hat{\mathbf{i}}+\frac{\sqrt{3}}{2}a_h\hat{\mathbf{j}},$$

$$\mathbf{B}_3^p=\frac{1}{2}a_h\hat{\mathbf{i}}+\frac{1}{3}\frac{\sqrt{3}}{2}a_h\hat{\mathbf{j}}+\frac{1}{3}c_h\hat{\mathbf{k}}, \qquad (3)$$

where a_h and c_h are the lattice constants, and $\hat{\mathbf{i}}$, $\hat{\mathbf{j}}$, and $\hat{\mathbf{k}}$ are dimensionless Cartesian unit vectors. The conventional $O3$ hexagonal cell corresponds to the stacking of three such slabs. The primitive unit cell defined by cell vectors $\mathbf{B}_i^p$ contains a single formula unit of the ternary compound. The unit-cell dimension normal to the layers is $c_h/3$, one-third the size of the conventional unit cell (cf. Fig. 3). One can obtain a four formula-unit cell, analogous to the monoclinic system with cell vectors $\mathbf{B}_i$, by doubling the first two cell vectors ($B_1=2B_1^p, B_2=2B_2^p$), while keeping the third unchanged ($B_3=B_3^p$).

An atomic coordinate $\mathbf{r}(j)=x(j)a\hat{\mathbf{i}}+y(j)a\hat{\mathbf{j}}+z(j)\frac{1}{3}c_h\hat{\mathbf{k}}$ in the Cartesian system can be written as

$$\mathbf{r}(j)=\left[x(j)+\frac{1}{\sqrt{3}}y(j)-\frac{2}{3}z(j)\right]\mathbf{B}_1^p+\left[\frac{2}{\sqrt{3}}y(j)-\frac{1}{3}z(j)\right]\mathbf{B}_2^p+z(j)\mathbf{B}_3^p \qquad (4)$$

in the primitive hexagonal system.

The layer z-coordinates are $z(\mathrm{Mn})=0$, $z(\mathrm{Li})=0.5$, $z(\mathrm{O}_1)=1-3z_0$, $z(\mathrm{O}_2)=3z_0$, in units of $c_h/3$, where the two oxygen layers are labeled O_1, and O_2. The internal coordinate z_0 is typically[29] about 0.25.

The transition-metal-layer atomic coordinates in the unit cell defined by $\mathbf{B}_i$ are taken to be (0,0,0), $(\frac{1}{2},0,0)$, $(0,\frac{1}{2},0)$, and $(\frac{1}{2},\frac{1}{2},0)$. The layer stacking follows the *ABC ABC* sequence, characteristic of cubic close-packing. In-plane coordinates of layer *B*, for example, are shifted by $(\frac{1}{3},\frac{2}{3},0)$ relative to those for layer *A*.

E. Relation between monoclinic and rhombohedral structures

The layered rhombohedral structure of $\mathrm{LiMnO_2}$ may be viewed as a special case of the monoclinic structure, in which the monoclinic distortions vanish, which occurs when

$$a_m = \sqrt{3}\, b_m, \tag{5}$$

and

$$c_m \cos\beta = -a_m/3, \tag{6}$$

and the hexagonal layer lattice constant $a_h = b_m = a_m/\sqrt{3}$.

F. Calculation parameters

The 16-atom-cell calculations utilized special k-points generated by Monkhorst-Pack[30] indices (4,4,4). Plane-wave energy cutoffs of 495 eV were employed in most of the calculations. The use of a high-precision basis enables accurate cell-parameter relaxations to be performed using the stress tensor. We employed the harder of the two ultrasoft Li pseudopotentials provided in the VASP pseudopotential library, designated Li_h, because in some instances a fully equilibrated atomic configuration was not obtainable with the softer Li pseudopotential.

G. Relaxation procedure

Both internal coordinates and cell coordinates were relaxed for each system. The internal coordinate relaxations employed the Hellmann-Feynman forces. The cell coordinates were relaxed, keeping the crystal symmetry (either rhombohedral or monoclinic) fixed, to reduce absolute values of stress tensor elements to small values, below about 10 kB. By this procedure, independent calculations for either the rhombohedral or the monoclinic crystal structure can be performed even when one of the structures is, in principle, unstable with respect to transformation to the other.

The initial atomic coordinate sets and lattice parameters for each doped system, employed at the outset of the relaxation process, were taken from the equilibrium results for the corresponding undoped ($\mathrm{LiMnO_2}$) system. Although this appears to be the most unbiased choice, there is no guarantee that downhill relaxation from these initial configurations will yield the only equilibrium configuration, particularly in the case of the relatively low-symmetry monoclinic structure. A metastable minimum was found for Co dopants in monoclinic $\mathrm{LiMnO_2}$. In the case of Co dopants, the ground-state configuration was obtained by adopting initial atomic coordinates in which the Jahn-Teller distortion of the solute-centered octahedron was suppressed. In the case of Fe dopants, the ground state corresponds to a high-spin configuration, and the initial atomic magnetic moment was set at $5\mu_B$. Low values of the initial Fe magnetic moment were found to result in spurious metastable intermediate-spin states.

III. RESULTS

A. Pristine system

Calculations for the rhombohedral structure with a ferromagnetic spin configuration as well as for the monoclinic structure with either a ferromagnetic or antiferromagnetic spin configuration yielded results in close agreement with those given by Mishra and Ceder,[15] who also employed VASP.

B. Dopant oxidation state

As mentioned earlier, simple arguments suggest that the effectiveness of a given dopant in stabilizing (destabilizing) the rhombohedral (monoclinic) structure is determined largely by its oxidation state.[10] To test this hypothesis, one must establish the oxidation state of different solutes in the rhombohedral and monoclinic phases of $\mathrm{LiMnO_2}$.

In principle, Mulliken population analysis or charge (or spin[31]) density integration provide the most direct way to extract transition metal oxidation states. Alternatively, analysis of local densities of electronic states and metal-oxygen bond lengths also give signatures of the oxidation state. None of these approaches gives results entirely free of ambiguity (nor do XANES measurements[10]). In the following, we analyze electronic spectra and Jahn-Teller coordinates to assign oxidation states of dopants in the monoclinic structure, and metal-oxygen bond lengths to determine oxidation states in the rhombohedral structure. For most of the dopants considered, the predominant valence is identifiable by these means. In the case of Co, a trivalent state is predicted in the monoclinic structure, but a divalent state occurs in the rhombohedral structure.

1. Monoclinic structure

In the monoclinic structure, the *d*-electron density-of-states spectra of Mn ions that are near neighbors of the substituted transition metal ion provides the clearest signature of the oxidation state.[32] The Mn-ion density of states spectra in this structure almost invariably exhibit empty minority band, fully occupied majority t_{2g} band, and either an empty majority e_g band for oxidation state 4+ or a half-filled Jahn-Teller-effect-split e_g band for oxidation state 3+. When a substitutional dopant in monoclinic $\mathrm{LiMnO_2}$ adopts the oxidation state of 2+, one of its near-neighbor Mn ions is oxidized to the 4+ state. This is illustrated in Fig. 4 for the case of a Cu dopant. The figure plots *d*-electron densities of states for majority (solid line) and minority (dashed line) bands; the Fermi level is at zero energy. The bottom panel shows the density of states for an Mn atom that is oxidized to 4+ by proximity to a Cu neighbor, and consequently has an empty majority e_g

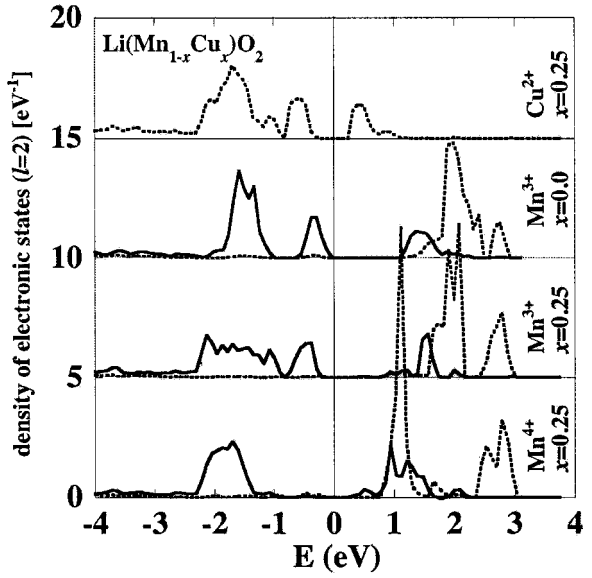

FIG. 4. Projected ($l=2$) density of electronic states for Mn and Cu ions calculated for the antiferromagnetic state of monoclinic $LiMn_{1-x}Cu_xO_2$. The full curves correspond to the majority spin, and the dashed curves, the minority spin bands. The top panel shows results for the minority spin of Cu. The second panel shows the density of states for Mn in the undoped system. The bottom two panels show spectra for Mn ions that are neighbors of the Cu dopant. One neighbor adopts a 4+ oxidation state, while the others remain in the 3+ state of the undoped system.

band. The second panel (shifted by 5 units) shows the density of states for the unoxidized Mn^{3+} neighbors, which may be compared with those for Mn ions in the pristine system, shown in the third panel. The top panel shows the density of states for the minority Cu^{2+} band, in which one of the e_g levels is unoccupied. Similar considerations enable us to identify transition metal solute oxidation states $M^{Z+}=Sc^{3+}$, Ti^{3+}, V^{3+}, Cr^{3+}, Fe^{3+}, Co^{3+}, and Ni^{2+}, in the monoclinic structure. These oxidation state assignments are consistent with Jahn-Teller-distortion analysis described below.

2. Rhombohedral structure

In undoped ferromagnetic rhombohedral $LiMnO_2$, a hypothetical system not found in nature, the Mn-ion density-of-states spectra (Fig. 5) does not show the stereotypical form observed for the monoclinic structure, and an intermediate rather than a high-spin state is predicted. In this case, the spin splitting is reduced sufficiently so that the minority t_{2g} spin band is one-third occupied. This behavior is evidence of the frustrated character of the 3+ oxidation state of Mn in the rhombohedral structure of $LiMnO_2$. (We note that the position of the *d*-bands would be shifted in a formulation in which on-site correlations are accounted for, such as the GGA+U method.[16])

The high symmetry of the rhombohedral structure, in which the six M—O bond lengths of each transition metal octahedron are closely similar, suggests the possibility of identifying dopant oxidation states by comparing bond lengths with predictions based on tabulated ionic radii. In

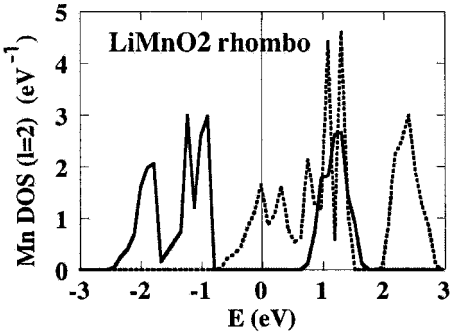

FIG. 5. Projected ($l=2$) Mn ion density of electronic states calculated for the ferromagnetic state of rhombohedral $LiMnO_2$, a hypothetical system. The usual high-spin state of Mn^{3+} does not occur in this system. In $LiMn_{0.5}Ni_{0.5}O_2$, in which the rhombohedral structure is stabilized, Mn avoids the unfavorable 3+ state and is oxidized to 4+.

Fig. 6, the abscissa represents the average M—O bond length calculated with the VASP code for dopant ions M in rhombohedral ferromagnetic $LiMn_{0.75}M_{0.25}O_2$, and the ordinate represents the sum of the empirical transition metal ionic radius[33] for a given oxidation state at a sixfold coordinated site, and an additive constant of 1.36 Å, the ionic radius of threefold coordinated O^{2-}. The latter choice appears most appropriate, although the O ions are threefold coordinated both to M and to Li (cf. Fig. 3). For the transition

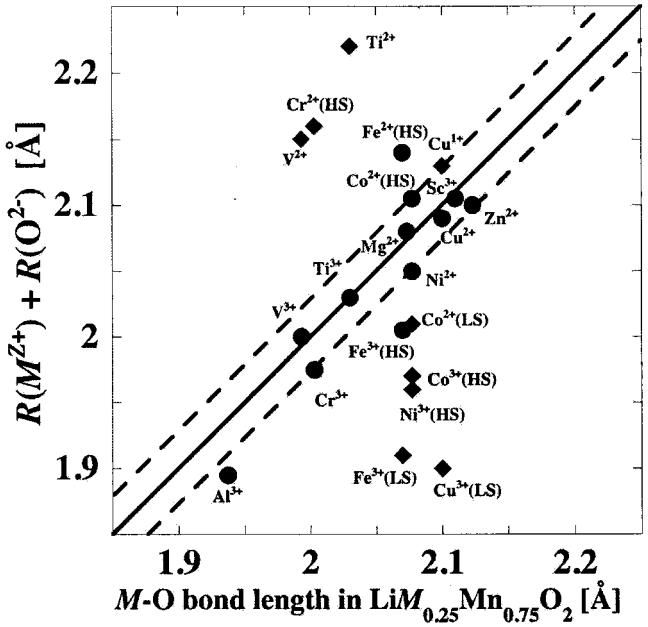

FIG. 6. The sum of (i) the empirical ionic radius for an octahedrally coordinated solute ion M in a hypothetical oxidation state, and (ii) the oxygen ionic radius, are plotted on the ordinate; average solute-oxygen bond length, calculated by first-principles methods for selected solutes in rhombohedral $LiMn_{0.75}M_{0.25}O_2$, is plotted on the abscissa. Filled circles correspond to oxidation states for which empirical values and first-principles calculations are in best agreement, whereas filled diamonds represent other hypothetical oxidation states. The solid line represents the limit of exact agreement between the first-principles and empirical values.

metal ions, empirical ionic radii for selected divalent and trivalent oxidation states are plotted. For several transition metal oxidation states, the ionic radii are different for high and low spin states.[33] In Fig. 6, we show for comparison several high spin and low spin radii.

The solid diagonal line in Fig. 6 represents the limit in which the calculated M—O bond lengths are equal to those predicted from standard ionic radii. The filled circles correspond to oxidation states for which calculated bond lengths are most consistent with empirical ionic radii, whereas the filled diamond symbols correspond to other, hypothetical, oxidation states, for which the calculated bond lengths are less consistent with the empirical ionic radii. The points denoted by filled circles mostly lie within the band bounded by the dashed lines, which represent a scatter of about one per cent. The transition-metal oxidation states deduced from Fig. 6 for rhombohedral $LiMn_{1-x}M_xO_2$ are Sc^{3+}, V^{3+}, Cr^{3+}, Co^{2+}, Ni^{2+}, and Cu^{2+}. The Fe bond length is located between those predicted for divalent and trivalent high-spin states. Fe is therefore in a lower oxidation state than in the monoclinic structure, in which it is unambiguously trivalent.

3. Comparison of dopant oxidation states in rhombohedral and monoclinic structures

Analyses in the preceding two sections have yielded predictions of the predominant oxidation states of selected dopants in monoclinic and rhombohedral $LiMn_{1-x}M_xO_2$. The results of these analyses indicate that transition elements earlier than Fe are trivalent and those later than Co are divalent, regardless of whether the structure is monoclinic or rhombohedral. This behavior reflects the trend of increasing effective third ionization potential with atomic number across the transition series. Co is predicted to be divalent in the rhombohedral structure but trivalent in the monoclinic structure. The former prediction appears to be consistent with experiment.[10] It would be of interest to determine whether the predictions for Co and Fe are borne out experimentally or in higher-level (e.g., GGA+U) calculations.

C. Jahn-Teller distortion in monoclinic structure

The oxygen octahedra that enclose Mn in monoclinic $LiMnO_2$ exhibit the polar-axis elongations characteristic of the Jahn-Teller effect for Mn^{3+}. The magnitude of this elongation is proportional to the amplitude Q_3 of the E_g (Jahn-Teller-active) frozen-phonon mode,

$$Q_3 = [2u_z(6) - 2u_z(3) - u_x(1) + u_x(4) - u_y(2) + u_y(5)]/\sqrt{12}, \tag{7}$$

where the six octahedral oxygen atoms are numbered as in Fig. 4 of Marianetti *et al.*:[34] atoms 3 and 6 are aligned along the z-axis in the positive and negative directions respectively, and atoms 1 and 4 (2 and 5) are aligned along the x (y) axes. Either a host Mn or a solute atom M is located at the origin. The quantities $u_i(j)$ refer to atomic displacements (or bond-length changes) with respect to an undistorted octahedron, whose reference Mn—O (or M—O) bond lengths are taken to be 1.98 Å, the bond length in rhombohedral $LiMnO_2$.

Insight may be gained into the structural distortions induced by solute atoms in the $C2/m$ variant of $LiMnO_2$ by analysis of Q_3. In each doped 16-atom unit cell are four metal-centered octahedra, one associated with solute M and three associated with host Mn atoms. The numerical values of the coordinates Q_1, Q_2, and Q_3 for host- and solute-centered octahedra are listed in Tables I (trivalent solutes), and II (Co and divalent solutes). Calculated values of Q_3 for Mn-centered octahedra are plotted in Fig. 7 against

$$Q_1 = [u_x(1) - u_x(4) + u_y(2) - u_y(5) + u_z(3) - u_z(6)]/\sqrt{6}, \tag{8}$$

the breathing-mode coordinate.

The filled symbols circumscribed by the circle in the lower left-hand corner correspond to Mn ions that are oxidized to the 4+ state by virtue of their proximity to an M^{2+} ion, whereas those enclosed in the circle at the upper-right-hand corner correspond to Mn^{3+}. The center of the circle that encloses the Mn^{3+} coordinates corresponds to the (Q_1, Q_3) coordinates for monoclinic $LiMnO_2$, whereas that for the Mn^{4+} coordinates corresponds to the (Q_1, Q_3) coordinates of rutile MnO_2; Mn in monoclinic $LiMnO_2$ and rutile MnO_2 may be considered reference systems for the trivalent and quadrivalent oxidation states, respectively. The Q_3 values in the reference systems essentially provide upper and lower bounds for the Q_3 values in the doped systems. One suspects that the oxidation states of Mn in the doped systems are either slightly reduced with respect to 4+ or slightly oxidized with respect to 3+, but further analysis would be required to verify that hypothesis.

In Fig. 8 are plots of the (Q_1, Q_3) coordinates for the various solutes under consideration, evaluated for both the monoclinic (diamond symbols) and rhombohedral (filled circles) structures. In the case of Co solutes in the monoclinic structure, a metastable divalent configuration is indicated by a square symbols. As mentioned above, two different Co configurations may be reached by adopting different starting configurations for the downhill relaxation procedure: the starting atomic configuration based on undoped $LiMnO_2$ relaxes to the metastable divalent configuration, but a starting configuration based the relaxed atomic coordinates for $LiCr_{0.25}Mn_{0.75}O_2$ [for which $Q_3(M)$ is small] yields the low energy atomic configuration upon relaxation, with Co trivalent.

The coordinate

$$Q_2 = [u_x(1) - u_x(4) - u_y(2) + u_y(5)]/2, \tag{9}$$

which couples to partially filled t_{2g}-bands, exhibits relatively small values, since these bands are either full or empty for the majority- and minority-spin bands in the $LiMnO_2$ host system; and essentially vanishing Q_2 values occur for the Mn octahedra.

As shown in Fig. 8, the non-Jahn-Teller-active trivalent ions Sc, Cr, Fe, Al, etc., all exhibit relatively low values of Q_3, compared to the Jahn-Teller active ions. That these Q_3 values are nevertheless nonzero reflects a competition between solute ion and the host environment of the monoclinic $LiM_{0.25}Mn_{0.75}O_2$ structure to optimize the configuration of

TABLE I. Coordinates Q_1, Q_2, and Q_3, in Å, of octahedra in monoclinic $LiMn_{0.75}M_{0.25}O_2$, for trivalent solutes M. Four octahedra, centered on either Mn or M, listed for each system.

System	Octahedron	Oxidation state	Q_1	Q_2	Q_3
$LiMnO_2$	Mn	3+	0.24	−0.01	0.49
$LiMn_{0.75}Al_{0.25}O_2$	Al	3+	−0.06	−0.00	0.12
$LiMn_{0.75}Al_{0.25}O_2$	Mn	3+	0.23	−0.03	0.44
$LiMn_{0.75}Al_{0.25}O_2$	Mn	3+	0.23	−0.01	0.48
$LiMn_{0.75}Al_{0.25}O_2$	Mn	3+	0.23	−0.03	0.44
$LiMn_{0.75}Sc_{0.25}O_2$	Sc	3+	0.36	0.00	0.16
$LiMn_{0.75}Sc_{0.25}O_2$	Mn	3+	0.28	−0.02	0.46
$LiMn_{0.75}Sc_{0.25}O_2$	Mn	3+	0.25	−0.01	0.48
$LiMn_{0.75}Sc_{0.25}O_2$	Mn	3+	0.27	−0.04	0.45
$LiMn_{0.75}Ti_{0.25}O_2$	Ti	3+	0.06	−0.01	0.04
$LiMn_{0.75}Ti_{0.25}O_2$	Mn	3+	0.31	−0.05	0.46
$LiMn_{0.75}Ti_{0.25}O_2$	Mn	3+	0.29	−0.02	0.47
$LiMn_{0.75}Ti_{0.25}O_2$	Mn	3+	0.37	−0.07	0.36
$LiMn_{0.75}V_{0.25}O_2$	V	3+	0.08	−0.01	0.10
$LiMn_{0.75}V_{0.25}O_2$	Mn	3+	0.25	−0.01	0.48
$LiMn_{0.75}V_{0.25}O_2$	Mn	3+	0.24	−0.01	0.47
$LiMn_{0.75}V_{0.25}O_2$	Mn	3+	0.24	−0.05	0.43
$LiMn_{0.75}Cr_{0.25}O_2$	Cr	3+	0.07	0.00	0.07
$LiMn_{0.75}Cr_{0.25}O_2$	Mn	3+	0.24	−0.02	0.44
$LiMn_{0.75}Cr_{0.25}O_2$	Mn	3+	0.24	−0.01	0.46
$LiMn_{0.75}Cr_{0.25}O_2$	Mn	3+	0.21	−0.04	0.40
$LiMn_{0.75}Fe_{0.25}O_2$	Fe	3+	0.21	−0.01	0.21
$LiMn_{0.75}Fe_{0.25}O_2$	Mn	3+	0.23	−0.01	0.44
$LiMn_{0.75}Fe_{0.25}O_2$	Mn	3+	0.24	−0.01	0.49
$LiMn_{0.75}Fe_{0.25}O_2$	Mn	3+	0.24	−0.03	0.47

oxygen ligands. We note that in rhombohedral $LiMnO_2$, the crystal symmetry essentially excludes Jahn-Teller distortion, and Q_3 values are close to zero for all solute ions.

D. Effect of solutes on relative stability of monoclinic and rhombohedral structures

Doping tends to destabilize the cooperative Jahn-Teller distortion in the monoclinic layered structure of $LiMnO_2$ in favor of the more symmetrical rhombohedral structure. We can assess the relative strength of this tendency for different solutes by comparing total energies calculated in both the rhombohedral and monoclinic structures. In Fig. 9, we plot the relative energy difference $\Delta E_{rm}(x=0.25)/E_{rm}(0)$, where $\Delta E_{rm}(x)$ is the difference in total energy between rhombohedral and monoclinic phases of $LiM_xMn_{1-x}O_2$. A positive value of $\Delta E_{rm}(x)$ indicates that the monoclinic phase is the more stable one at that composition. The results in the figure show that at $x=0.25$, none of the dopants is predicted to stabilize the rhombohedral structure. A linear extrapolation of the results, however,

$$x_{rm} = x_1 \Delta E_{rm}(0)/(-\Delta E_{rm}(x_1) + \Delta E_{rm}(0)), \qquad (10)$$

where $x_1=0.25$, predicts that the critical concentration x_{rm} lies in the range of 0.3–0.4 for the divalent dopants. In view of the higher values of $\Delta E_{rm}(x=0.25)/E_{rm}(0)$ for trivalent ions, determination of x_{rm} by this relation would require a wide extrapolation. The greater tendency of divalent solutes to stabilize the rhombohedral structure, however, is clear.

One observes an overall trend toward increasing rhombohedral stabilization as one traverses the transition series from earlier to later elements. Filled shell divalent solutes have the greatest stabilizing effect, whereas filled shell trivalent solutes have the least stabilizing effect; solutes with partially filled shells lie in between. In this context, Co^{3+} and Ni^{2+} in the monoclinic structure are regarded as filled-shell ions; Ni, for example, has a filled majority band and filled minority t_{2g} band.

IV. DISCUSSION

A. Influence of oxidation state on x_{rm}

According to an approximate empirical rule[35] obeyed by $Li_{1+x}Mn_{2-x}O_4$ spinels ($0<x<0.33$), cooperative Jahn-Teller distortions occur when the fraction of Mn^{3+} on the transition-metal sublattice is greater than half. The rule is based on the assumption that the oxidation state is the predominant feature that determines whether the cooperative Jahn-Teller distortion occurs. If applied without modification to layered

TABLE II. Coordinates, Q_1, Q_2, and Q_3, in Å, of octahedra in monoclinic $LiMn_{0.75}M_{0.25}O_2$, for divalent solutes M and Co. Two equilibrium configurations are listed for Co, the first of which Corresponds to the trivalent ground state configuration, and the second to a metastable divalent configuration.

System	Octahedron	Oxidation state	Q_1	Q_2	Q_3
$LiMn_{0.75}Co_{0.25}O_2$	Co	3+	−0.03	0.00	0.02
$LiMn_{0.75}Co_{0.25}O_2$	Mn	3+	0.21	−0.03	0.42
$LiMn_{0.75}Co_{0.25}O_2$	Mn	3+	0.22	−0.01	0.47
$LiMn_{0.75}Co_{0.25}O_2$	Mn	3+	0.20	−0.03	0.41
$LiMn_{0.75}Co_{0.25}O_2$	Co	2+	0.23	−0.03	0.48
$LiMn_{0.75}Co_{0.25}O_2$	Mn	4+	−0.02	−0.02	0.15
$LiMn_{0.75}Co_{0.25}O_2$	Mn	3+	0.22	−0.04	0.48
$LiMn_{0.75}Co_{0.25}O_2$	Mn	3+	0.20	−0.02	0.42
$LiMn_{0.75}Ni_{0.25}O_2$	Ni	2+	0.26	−0.04	0.18
$LiMn_{0.75}Ni_{0.25}O_2$	Mn	4+	−0.10	−0.01	0.02
$LiMn_{0.75}Ni_{0.25}O_2$	Mn	3+	0.21	−0.05	0.44
$LiMn_{0.75}Ni_{0.25}O_2$	Mn	3+	0.22	−0.02	0.45
$LiMn_{0.75}Cu_{0.25}O_2$	Cu	2+	0.41	−0.05	0.53
$LiMn_{0.75}Cu_{0.25}O_2$	Mn	4+	−0.09	0.00	0.01
$LiMn_{0.75}Cu_{0.25}O_2$	Mn	3+	0.25	−0.07	0.51
$LiMn_{0.75}Cu_{0.25}O_2$	Mn	3+	0.21	0.00	0.44
$LiMn_{0.75}Mg_{0.25}O_2$	Mg	2+	0.24	−0.05	0.19
$LiMn_{0.75}Mg_{0.25}O_2$	Mn	4+	−0.08	−0.01	0.01
$LiMn_{0.75}Mg_{0.25}O_2$	Mn	3+	0.23	−0.04	0.46
$LiMn_{0.75}Mg_{0.25}O_2$	Mn	3+	0.19	−0.01	0.35
$LiMn_{0.75}Zn_{0.25}O_2$	Zn	2+	0.35	−0.05	0.20
$LiMn_{0.75}Zn_{0.25}O_2$	Mn	4+	−0.07	0.00	0.01
$LiMn_{0.75}Zn_{0.25}O_2$	Mn	3+	0.25	−0.05	0.47
$LiMn_{0.75}Zn_{0.25}O_2$	Mn	3+	0.21	0.00	0.37

structures, the rule would imply that $x_{rm}=0.25$ for divalent and $x_{rm}=0.5$ for trivalent solutes. This simple rule somewhat overestimates the Jahn-Teller-distortion-suppressing properties of solutes compared to our first-principles LSDA-GGA predictions for zero temperature.

The empirical rule neglects several effects, including (i) atomic-size differences between dopants and host atoms, (ii) magnetic properties of the dopants, (iii) dopant covalency, (iv) oxygen participation in the charge transfer induced by dopants, (v) competition between dopant atoms and Mn for optimal coordination with shared oxygen neighbors, and (vi) electronic subshell filling, all of which may influence x_{rm}. Features (i)–(v) are difficult to analyze separately, however, Fig. 9 shows that within the classes of divalent or trivalent dopants, the relative degree of stabilization correlates with whether or not the t_{2g} or e_g subshells are partially filled. This behavior is plausible, in that an element with a partially filled e_g subshell (Cu) is Jahn-Teller active in the same sense as Mn, and therefore more compatible with the host $C2/m$ structure than filled-shell systems with the same oxidation state. Similarly, elements with partially filled t_{2g} shells (Ti, V) have Jahn-Teller activity that is incompatible with the host structure, and therefore are more effective in destabilizing that structure than filled-shell systems with the same oxidation state. The filled-shell trivalent ions Al, Sc, and Cr are least effective in stabilizing the rhombohedral structure. Fe does not immediately conform to this interpretation, because in its adopted trivalent high-spin configuration (5 spin-up, zero spin-down electrons) in the monoclinic structure, it is a filled shell ion in the same sense as Sc and Cr. It is possible that the mixed-valent character of Fe in the rhombohedral structure, however, which promotes the oxidation of Mn^{3+}, enhances its ability to stabilize that structure.

Nitrogen solutes (cf. point on far left of the abscissa scale of Fig. 9) that substitute for oxygen in effect introduce closed-shell "dopants" Mn^{4+} on the Mn sublattice. The N-substituted system is therefore, in a sense, analogous to those with trivalent closed-shell dopants, which eliminate a single Mn^{3+} ion per dopant. Nitrogen, however, also distorts the ligand sublattice and it therefore stabilizes the rhombohedral structure to a greater extent than the trivalent closed-shell dopants.

B. Influence of temperature on x_{rm}

The LSDA-GGA treatment employed in this work is a zero-temperature approximation. Comparisons of such zero-temperature calculations with experiments, typically done at room temperature, must therefore be regarded with caution. At room temperature, the magnetic configurations are pre-

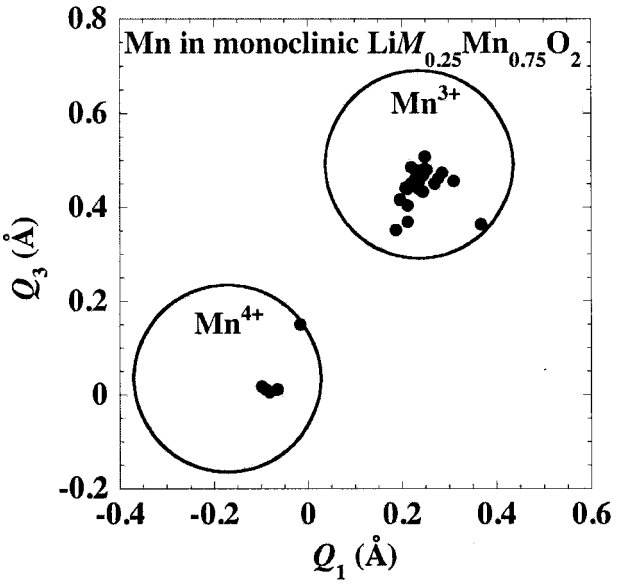

FIG. 7. Amplitude of Jahn-Teller active frozen-phonon mode Q_3 as a function of breathing mode coordinate Q_1 in monoclinic $LiMn_{0.75}M_{0.25}O_2$ for Mn-centered oxygen octahedra. Results for M=Mg, Zn, Al and first transition series elements are superposed. Filled circles denote Mn-centered octahedra. The large circles, with radius 0.2 Å, are centered on the Jahn-Teller coordinates of Mn in quadrivalent (rutile MnO_2) and trivalent (monoclinic $LiMnO_2$) structures, respectively. These circles enclose the coordinates that correspond to Mn^{4+} and Mn^{3+} octahedra.

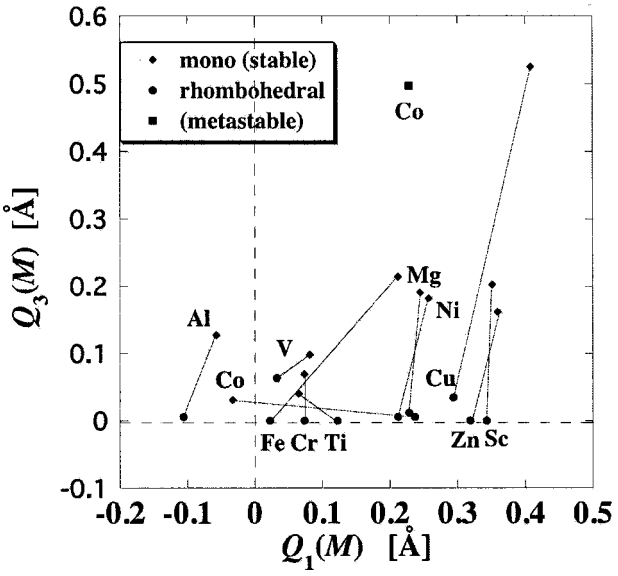

FIG. 8. Amplitude of Jahn-Teller active frozen-phonon mode Q_3 as a function of breathing mode coordinate Q_1 in monoclinic (filled diamonds), rhombohedral (filled circles) $LiMn_{0.75}M_{0.25}O_2$ for solute-centered oxygen octahedra. The filled squares represent metastable configurations for Co in the monoclinic structure, as discussed in the text. The metastable configuration of Co in the monoclinic structure is divalent; the stable configuration is trivalent. Results for solutes M=Mg, Ni, Co, Cu, Al, Fe, and Cr are shown.

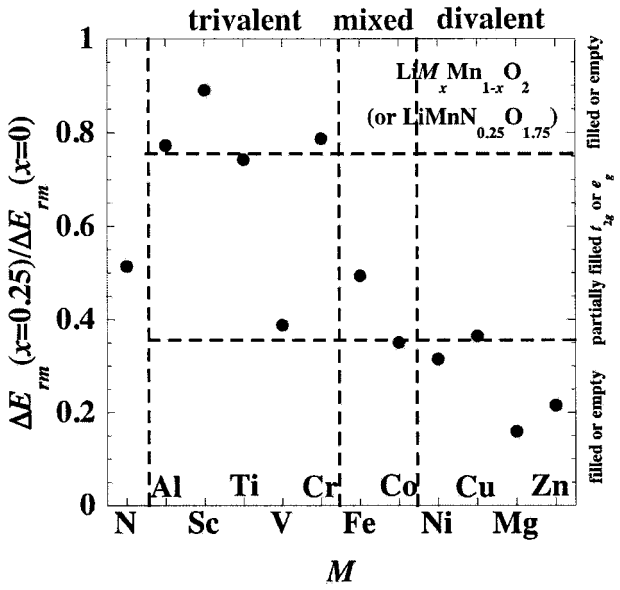

FIG. 9. Energy difference between rhombohedral and monoclinic phases at dopant concentration x=0.25, normalized by the energy difference for the undoped systems. Divalent dopants are more effective at stabilizing the rhombohedral structure than trivalent dopants. The stabilizing effect of a given dopant also correlates with the subshell filling.

sumably disordered,[7,24] with short-range correlations. Total (internal) energies in the limiting case of disordered local moments have been calculated within the coherent potential approximation for the Co doped system.[36] Most desirable would be the calculation of thermodynamic free energies as a function of temperature with short range magnetic correlations[37] and vibrational effects[38] included. Such a calculation for the present systems, however, would be a formidable task.

In general, one anticipates that

$$dx_{rm}/dT < 0, \tag{11}$$

since the free-energy change associated with temperature-driven magnetic and vibrational disorder should be larger for the symmetry-broken (monoclinic) phase. We suspect that the critical concentrations x_{rm} at room temperature may be reduced considerably, relative to their values at zero temperature. No experimental values of x_{rm}, however, are available for any of the systems addressed here, owing to the difficulty in synthesizing uniform, single-phase, fully lithiated specimens at a series of compositions.

C. Dopant selection

It is natural to inquire as to which of the dopants would be most suitable for practical Li-battery cathode materials based on layered rhombohedral $LiMn_{1-x}M_xO_2$. Our results indicate that the divalent dopants, such as Mg, Zn, etc., are most effective in suppressing the cooperative Jahn-Teller distortion. In practice, Ni, particularly at the composition $LiMn_{0.5}Ni_{0.5}O_2$, has been widely investigated. In the Li insertion/extraction cycling of this material, however, Ni

rather than Mn is the active species and cycles between 2+ and 4+ oxidation states.[39] The valence-skipping property of Ni $(2+ \leftrightarrow 4+)$ in $LiMn_{0.5}Ni_{0.5}O_2$ (Ref. 40) and $LiMn_{1/3}Ni_{1/3}Co_{1/3}O_2$ (Refs. 41 and 42) results in a higher capacity than a material based on Mn transitions between 3+ and 4+ would possess. The unfavorable Mn^{3+} oxidation state in the rhombohedral structure, remarked upon earlier, influences the cycling behavior of lightly doped rhombohedral $LiMn_{1-x}M_xO_2$, which transforms to the spinel structure upon delithiation.[11,12]

V. CONCLUSIONS

Early first-row transition-metal dopants are trivalent, whereas those later than Co divalent in either monoclinic or rhombohedral $LiMn_{1-x}M_xO_2$, with $x=0.25$. Co has a mixed-valent character, trivalent in the monoclinic and divalent in the rhombohedral structure. Total energy calculations indicate that the relative effectiveness of dopants in stabilizing the rhombohedral structure correlates first with the dopant oxidation state and, for a given oxidation state, with the t_{2g} or e_g subshell filling. The present results lend support to the view that divalent dopants are especially effective in suppressing the Jahn-Teller distortion because each dopant removes two Mn^{3+} ions from the transition metal sublattice, whereas trivalent dopants only remove one. For other reasons,[43] divalent dopants also turn out to be effective in suppressing the layered-spinel transformation upon delithiation.

ACKNOWLEDGMENTS

This work was supported at Argonne National Laboratory by the Chemical Sciences Division of the Office of Basic Energy Sciences, U.S. Department of Energy, under Contract No. W31-109-Eng-38, and at the Indian Institute of Technology, Kanpur, by the Council of Scientific and Industrial Research, New Delhi, under Scheme No. 03(968)02/EMR-II. Grants of computer time at the National Energy Research Supercomputer Center, Lawrence Berkeley Laboratory, and at the JAZZ cluster, Argonne National Laboratory, are gratefully acknowledged.

[1] J. M. Tarascon and M. Armand, Nature (London) **414**, 359 (2001).
[2] G. Dittrich and R. Hoppe, Z. Anorg. Allg. Chem. **368**, 262 (1969); R. Hoppe, G. Brachtel, and M. Jansen, *ibid.* **417**, 1 (1975).
[3] A. R. Armstrong and P. G. Bruce, Nature (London) **381**, 499 (1996).
[4] F. Capitaine, P. Gravereau, and C. Delmas, Solid State Ionics **89**, 197 (1996).
[5] A. R. Armstrong, R. Gitzendanner, A. D. Robertson, and P. G. Bruce, Chem. Commun. (Cambridge) **17**, 1833 (1998).
[6] S. T. Myung, S. Komaba, N. Hirosaki, and N. Kumagai, Electrochem. Commun. **4**, 397 (2002).
[7] Y. I. Jang, F. C. Chou, and Y. M. Chiang, J. Phys. Chem. Solids **60**, 1763 (1999).
[8] B. Ammundsen, J. Desilvestro, T. Groutso, D. Hassell, J. B. Metson, E. Regan, R. Steiner, and P. J. Pickering, J. Electrochem. Soc. **147**, 4078 (2000).
[9] Z. P. Guo, S. Zhong, G. X. Wang, H. K. Liu, S. X. Dou, J. Alloys Compd. **348**, 231 (2003).
[10] R. Prasad, R. Benedek, A. J. Kropf, C. S. Johnson, A. D. Robertson, P. G. Bruce, and M. M. Thackeray, Phys. Rev. B **68**, 012101 (2003).
[11] J. Reed, G. Ceder, and A. Van Der Ven, Electrochem. Solid-State Lett. **4**, A78 (2001).
[12] A. R. Armstrong, A. D. Robertson, and P. G. Bruce, Electrochim. Acta **45**, 285 (1999).
[13] G. Kresse and J. Furthmüller, Comput. Mater. Sci. **6**, 15 (1996); Phys. Rev. B **54**, 11 169 (1996).
[14] Y. Wang and J. P. Perdew, Phys. Rev. B **44**, 13 298 (1991).
[15] S. K. Mishra and G. Ceder, Phys. Rev. B **59**, 6120 (1999).
[16] A. Rohrbach, J. Hafner, and G. Kresse, J. Phys.: Condens. Matter **15**, 979 (2003).
[17] F. Zhou, C. A. Marianetti, C. Cococcioni, G. Morgan, and G. Ceder, Phys. Rev. B **69**, 201101 (2004).
[18] J. E. Greedan, N. P. Raju, and I. J. Davidson, J. Solid State Chem. **128**, 209 (1997).
[19] D. J. Singh, Phys. Rev. B **55**, 309 (1997).
[20] J. E. Greedan, N. P. Raju, A. S. Wills, C. Morin, S. Shaw, and J. N. Reimers, Chem. Mater. **10**, 3058 (1998).
[21] J. Rodriguez-Carvajal, G. Rousse, C. Masquelier, and M. Hervieu, Phys. Rev. Lett. **81**, 4660 (1998).
[22] A. S. Wills, N. P. Raju, and J. E. Greedan, Chem. Mater. **11**, 1510 (1999).
[23] A. S. Wills, N. P. Raju, C. Morin, and J. E. Greedan, Chem. Mater. **11**, 1936 (1999).
[24] M. E. Spahr, P. Novak, B. Schnyder, O. Haas, and R. Nesper, J. Electrochem. Soc. **145**, 1113 (1998).
[25] H. Kadowaki, H. Takei, and K. Motoya, J. Phys.: Condens. Matter **7**, 6869 (1995).
[26] T. A. Hewston and B. L. Chamberland, J. Phys. Chem. Solids **48**, 47 (1987).
[27] K. Takizawa and A. Hagiwara, J. Power Sources **109**, 127 (2002).
[28] C. Delmas, C. Fouassier, and P. Hagenmuller, Physica B & C **99**, 81 (1980).
[29] M. K. Aydinol, A. F. Kohan, G. Ceder, K. Cho, and J. Joannopoulos, Phys. Rev. B **56**, 1354 (1997).
[30] H. J. Monkhorst and J. D. Pack, Phys. Rev. B **13**, 5188 (1976).
[31] J. Reed and G. Ceder, Electrochem. Solid-State Lett. **5**, A145 (2002).
[32] In principle, the spectra for the dopant itself, of course, give equivalent information; however, the identification of the oxidation state for some transition metal ions would require not only a projection of the *d*-state spectra but a separate projection of the e_g and t_{2g} multiplets. The large multiplet splitting for Mn makes the identification of the spectra clear even without an explicit projection.

[33] R. D. Shannon, Acta Crystallogr., Sect. A: Cryst. Phys., Diffr., Theor. Gen. Crystallogr. **32**, 751 (1976).
[34] C. A. Marianetti, D. Morgan, and G. Ceder, Phys. Rev. B **63**, 224304 (2001).
[35] M. M. Thackeray, Prog. Solid State Chem. **25**, 1 (1997).
[36] A. I. Landa, C. C. Chang, P. N. Kumta, L. Vitos, and I. A. Abrikosov, Solid State Ionics **149**, 209 (2002).
[37] D. Morgan, B. Wang, G. Ceder, and A. van de Walle, Phys. Rev. B **67**, 134404 (2003).
[38] A. van de Walle and G. Ceder, Rev. Mod. Phys. **74**, 11 (2002).
[39] C. S. Johnson, J. S. Kim, A. J. Kropf, A. J. Kahaian, J. T. Vaughey, L. M. L. Fransson, K. Edstrom, and M. M. Thackeray, Chem. Mater. **12**, 2313 (2003).
[40] T. Ohzuku and Y. Makimura, Chem. Lett. **8**, 744 (2001).
[41] Z. Lu, D. D. MacNeil, and J. R. Dahn, Electrochem. Solid-State Lett. **4**, A200 (2001).
[42] T. Ohzuku and Y. Makimura, Chem. Lett. **7**, 642 (2001).
[43] J. Reed and G. Ceder, Chem. Rev. (Washington, D.C.) **104**, 4513 (2004).